

Electronic Supplementary Information

MoS₂/CoS₂ Heterostructures as Thermoelectric-catalyst for H₂O₂ Generation under Small Temperature Gradient

*Johnson Mary Leeda Rani Abisharani,^a Yangyang Wan,^b Qian Yu,^{*c,d} Yuyan Xu,^a Yinhua Jiang,^a Jun Qian,^a Shun Li,^a Li Li,^a Siew Yee Wong,^d Xu Li^{*d,e} and Jianming Zhang^{*a,d}*

^aSchool of Chemistry and Chemical Engineering, Jiangsu University, Zhenjiang, Jiangsu, 212013, China.
E-mail: zhangjm@ujs.edu.cn

^bSchool of Material Science and Engineering, Jiangsu University, Zhenjiang, Jiangsu, 212013, China

^cSchool of Life Sciences, Jiangsu university, Zhenjiang, Jiangsu, 212013, China.

^dInstitute of Materials Research and Engineering (IMRE), Agency for Science Technology and Research (A*STAR), Singapore 138634, Republic of Singapore.

^eInstitute of Sustainability for Chemicals, Energy and Environment (ISCE2), A*STAR, Singapore 627833, Republic of Singapore.

Materials

Thiourea ($\text{CH}_4\text{N}_2\text{S}$), Ammonium molybdate tetrahydrate ($(\text{NH}_4)_6\text{Mo}_7\text{O}_{24}\cdot 4\text{H}_2\text{O}$), Sodium hydroxide (NaOH), Cobalt nitrate hexahydrate ($\text{Co}(\text{NO}_3)_2\cdot 6\text{H}_2\text{O}$), and Sulphur powder were purchased from Shanghai Aladdin Biochemical Technology Co. Ltd and used without any further purification. Water was deionized and Millipore grade.

Preparation of $\text{MoS}_2/\text{CoS}_2$ heterostructure

The monocomponent MoS_2 and CoS_2 were synthesized according to literature report¹. The $\text{MoS}_2/\text{CoS}_2$ heterostructure was synthesized using a modified hydrothermal method. Typically, three different weight ratios of Ammonium molybdate tetrahydrate and Cobalt nitrate hexahydrate (elemental ratio of Mo:Co = 1:1, 2:3 and 3:2) were dissolved in 70 ml of deionized water. Additionally, a dual proportion of thiourea was added to the mixture, which was then stirred for 30 minutes and the pH value of 5 was maintained by adding appropriate amount of NaOH . This solution was then transferred to a Teflon autoclave and kept at 180°C for 24 hours. The resulting suspension was washed with water and ethanol three times and dried at 60°C for 12 hours in a vacuum oven. Finally, the $\text{MoS}_2/\text{CoS}_2$ heterostructure was obtained by sulfurizing the product using Sulfur in a tubular furnace under N_2 flow at 500°C , with a ramp rate of 5°C min^{-1} for 5 hours. The $\text{MoS}_2/\text{CoS}_2$ heterostructures were denoted based on Mo:Co elemental ratios as 3:1, 2:3, and 3:2 respectively.

TE catalytic reaction

In a typical reaction setup, 50 mg of the TE catalyst was dispersed and sonicated in 50 ml of deionized water to form a uniform suspension in a beaker, which was heated in an oil bath under magnetic stirring, while a temperature gradient across the solution was created by placing a cooling coil tube (cooling water temperature = 5°C , cycled using a chilling machine) into the solution. The temperature gradient can be facilely tuned by varying the oil bath temperature (25, 35, 45 and 55 K). The dynamics of heat transfer between the oil bath, chilling machine and the solution, resulting maintain temperature (20, 30, 40 and 50 K). O_2 was purged into the solution during the reaction test. At specified time intervals, 3 ml of the suspension was collected and filtrated with a $0.22\ \mu\text{m}$ filtration membrane to remove the catalyst. The H_2O_2 concentration was examined by iodometry method. A 100 mL aqueous solution containing KI (0.4 M), NaOH (0.6 M) and $(\text{NH}_4)_6\text{Mo}_7\text{O}_{24}\cdot\text{H}_2\text{O}$ (0.1 mM) was used as the solution A; solution B is an aqueous solution of 0.1 M $\text{C}_8\text{H}_5\text{KO}_4$. Afterward, 3 ml of the filtered solution was added to 0.5 ml of solutions A and B. The H_2O_2 reacted with I^- to generate I_3^- , which was then determined by measuring the absorbance

at 350 nm using UV-vis spectroscopy. The concentration of H_2O_2 was then calculated from the absorbance of the UV-Vis peak at 350 nm.

Electrochemical measurements

The electrochemical test was carried out in a three-electrode system in 0.1 M of Na_2SO_4 electrolyte solution using Pt as a counter electrode, Ag/AgCl as the reference electrode and catalyst coated on the copper foil as the working electrode, respectively. The working electrode was prepared by dispersing 50 mg of the nanoparticle sample in 1 ml ethanol and 80 μL of Nafion solution to form a slurry. Afterward, the slurry was coated onto a copper foil with an active area of $\sim 1 \text{ cm}^2$ and dried at 60 $^\circ\text{C}$ for 3 hrs. EIS was recorded in the frequency range of 0.01 Hz to 1000 kHz.

Characterization

A Rigaku D/max-2550 VB XRD was used to characterize the crystal structure of the synthesized materials. The morphology of the nanostructure was observed using JEOL-7800F SEM and a Talos F200X TEM with energy-dispersive spectrometer (EDX). XPS spectra was obtained using an ESCALAB 250 Xi spectrometer. FTIR was measured using a Nicole iS50 spectroscopy equipped with an in-situ catalysis measurement accessory (Shanghai LingLu Instruments). Ultraviolet-visible (UV-Vis) absorption spectra was analyzed with a UV-3600i Plus UV-Visible spectrometer. The electrochemical measurements were conducted using a CHI-660e station with a three-electrode system.

DFT calculation

First-principles calculations incorporating spin polarization were conducted within the Vienna Ab Initio Simulation Package (VASP) framework, employing the projector augmented-wave (PAW) pseudopotentials²⁻⁴. The exchange-correlation functional was treated through the Perdew-Burke-Ernzerhof (PBE) parameterization of the generalized gradient approximation⁵. To properly account for van der Waals forces, we implemented the DFT-D3⁶ dispersion correction scheme. Structural optimization of the $\text{CoS}_2/\text{MoS}_2$ heterostructure utilized a Monkhorst-Pack k-point mesh with $6 \times 2 \times 1$ divisions for Brillouin zone integration. Our computational setup specified a plane-wave energy cutoff of 500 eV, with convergence thresholds maintained at 10^{-5} eV for total energy and $0.03 \text{ eV} \cdot \text{\AA}^{-1}$ for atomic forces. A vertical vacuum spacing exceeding 15 \AA effectively suppressed artificial interlayer coupling along the z-direction. Post-processing and visualization tasks were accomplished using VASPKIT⁷ and VESTA⁸ software packages, respectively.

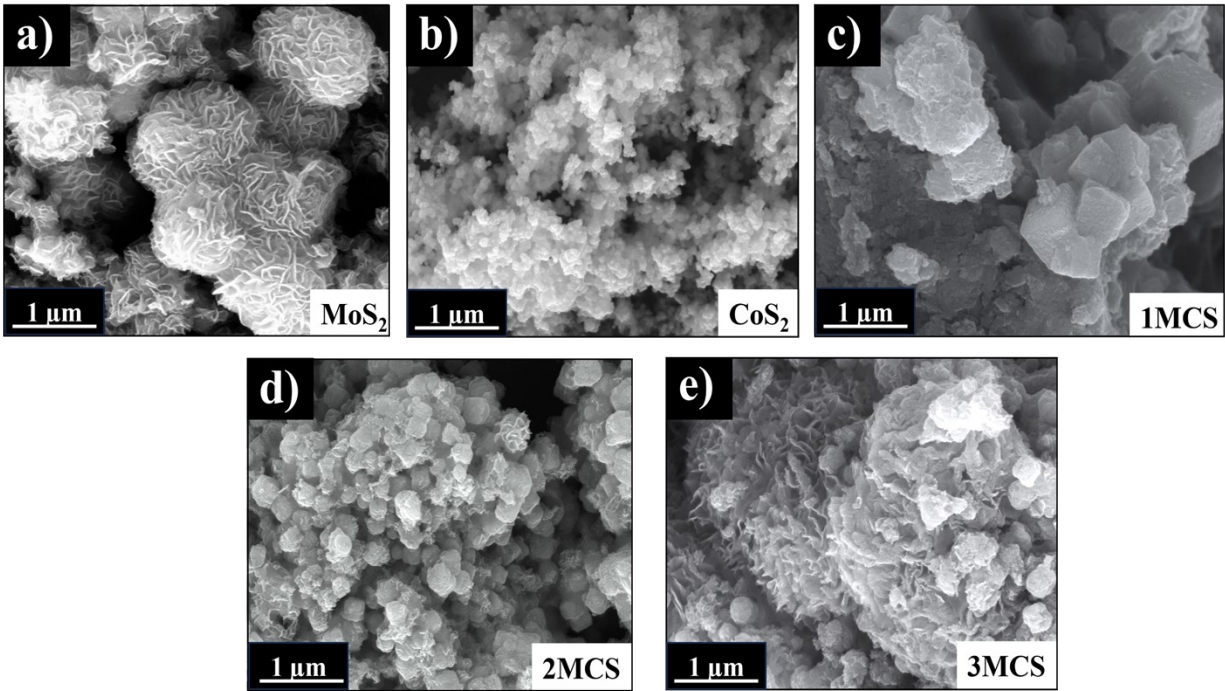


Fig. S1. SEM images of MoS₂, CoS₂, and MoS₂/ CoS₂ samples.

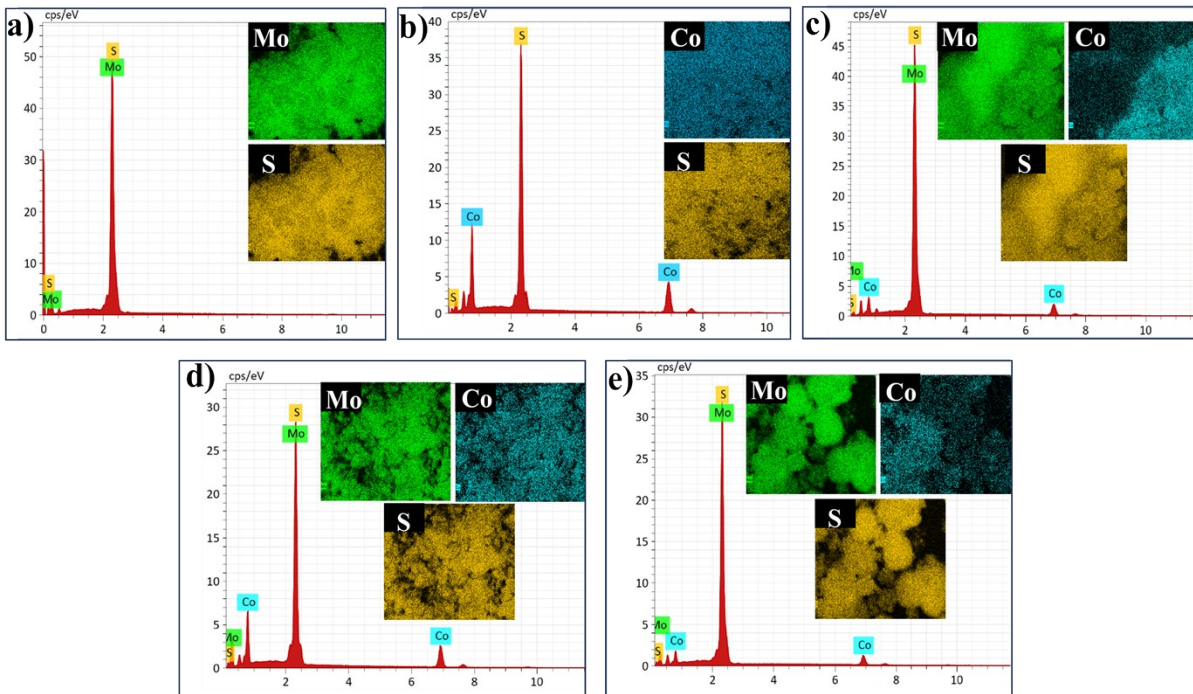


Fig. S2. EDX elemental mapping images of the catalyst samples. a) bare-MoS₂, b) bare-CoS₂, c) 1MCS, d) 2MCS and e) 3MCS.

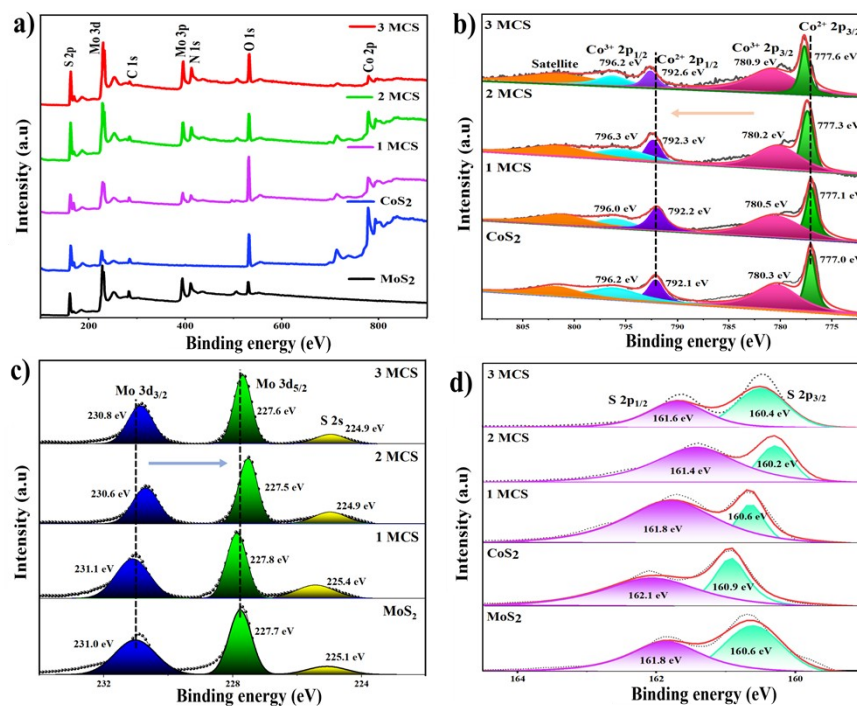


Fig. S3. a) XPS survey spectrum of MoS₂, CoS₂ and MoS₂/CoS₂. b) XPS spectra of Co 2p. c) XPS spectra of Mo 3d and d) XPS spectra of S 2p.

Fig. S4 a illustrates the interfacial model for DFT simulation. The electrostatic potential profiles indicate that the work function of metallic CoS₂ is 4.85 eV (**b**), while that of semiconducting MoS₂ is 5.44 eV (**c**). This difference drives spontaneous electron transfer from CoS₂ to MoS₂ upon an interface formation, as the system seeks Fermi level equilibrium. The planar-averaged charge density difference further confirms this phenomenon (**d**), revealing electron accumulation on the MoS₂ side and corresponding depletion on the CoS₂ side. This interfacial charge redistribution is visualized in the three-dimensional charge density difference isosurface (**e**), which distinctly shows net electron migration across the junction. These results confirm the formation of a Mott-Schottky heterojunction, in which the built-in electric field at the interface facilitates charge separation and modulates the local electronic environment. Such interfacial electronic reconstruction is expected to enhance the adsorption and activation of reaction intermediates, thereby contributing significantly to the improved electrocatalytic performance observed in the CoS₂/MoS₂ nano hybrid for surface catalysis.

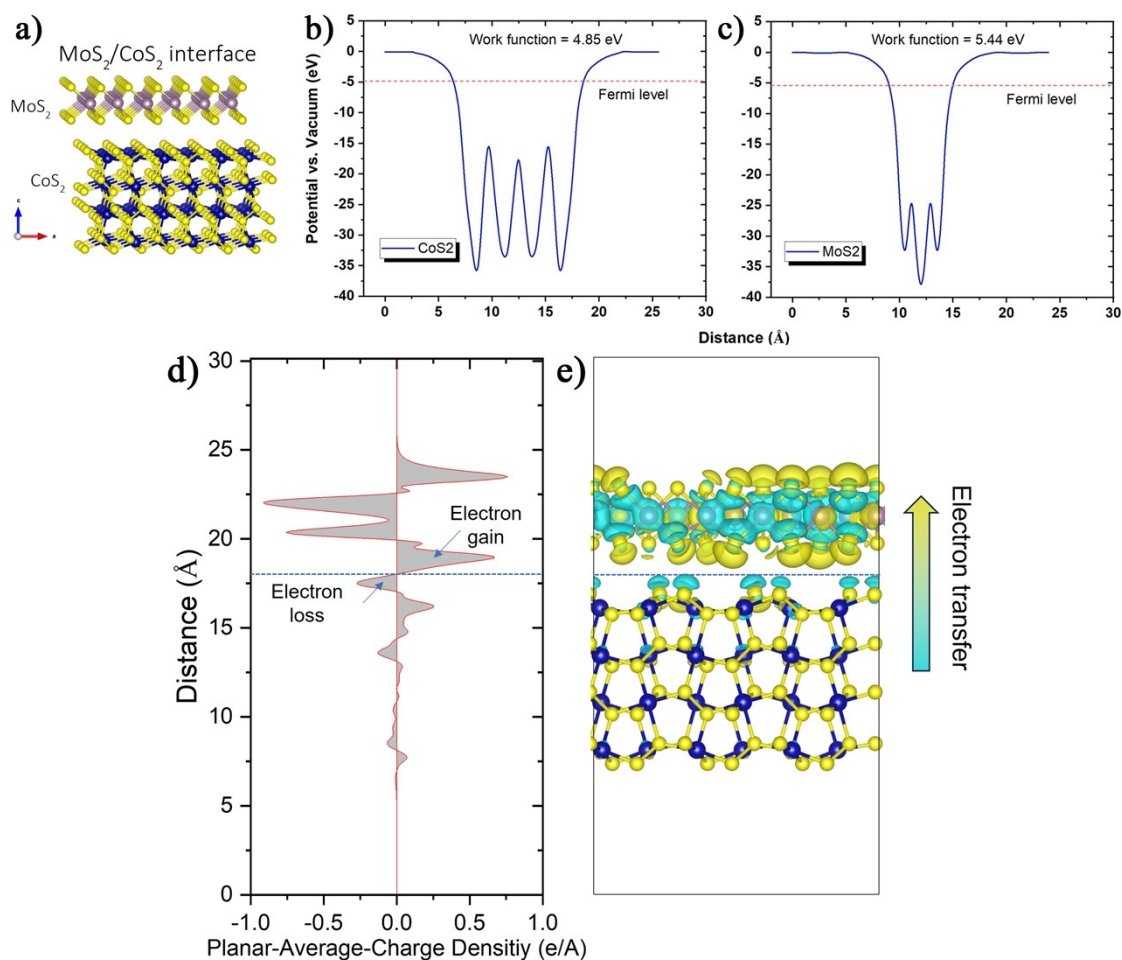


Fig. S4. (a) The MoS₂/CoS₂ interfacial model for DFT calculation. Electrostatic potential profiles of CoS₂ (b) and MoS₂ (c) monocomponents. (d) Planar-averaged charge density difference profiles (d) and three-dimensional charge density difference isosurface of the MoS₂/CoS₂ interface.

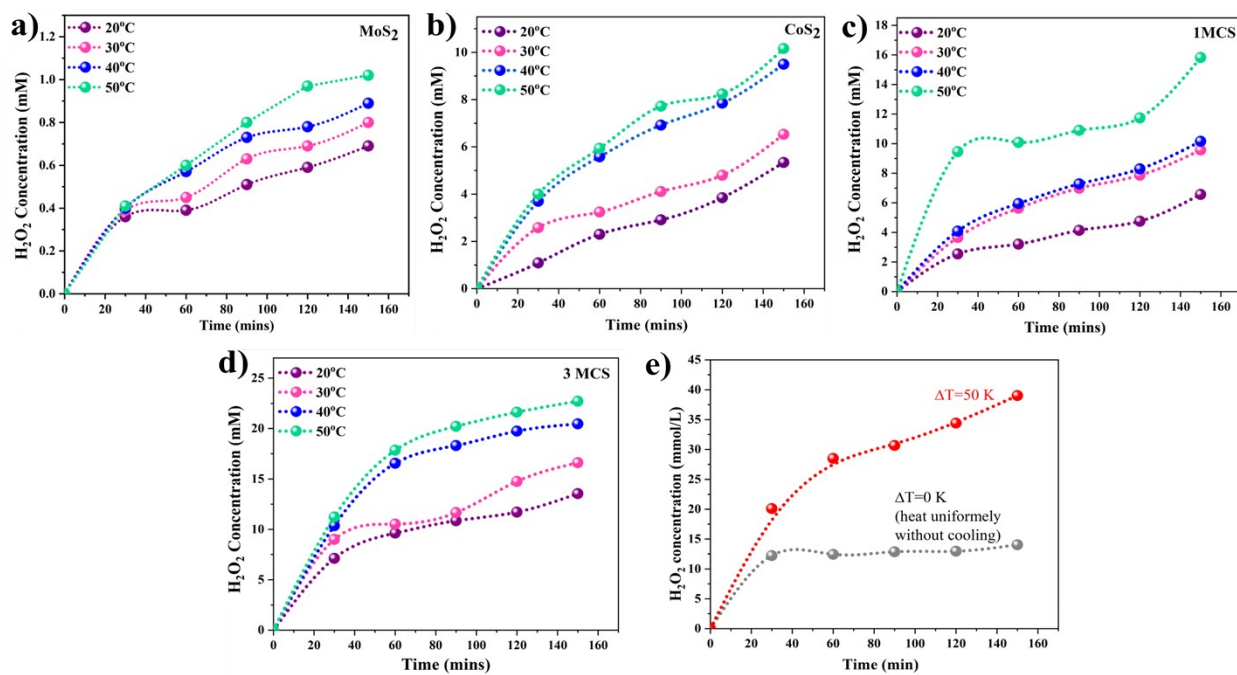


Fig. S5. (a-d) Temperature gradient H₂O₂ yield of TE catalyst performance at various temperature gradients. (e) Catalytic H₂O₂ generation of 2MCS with and without temperature gradient.

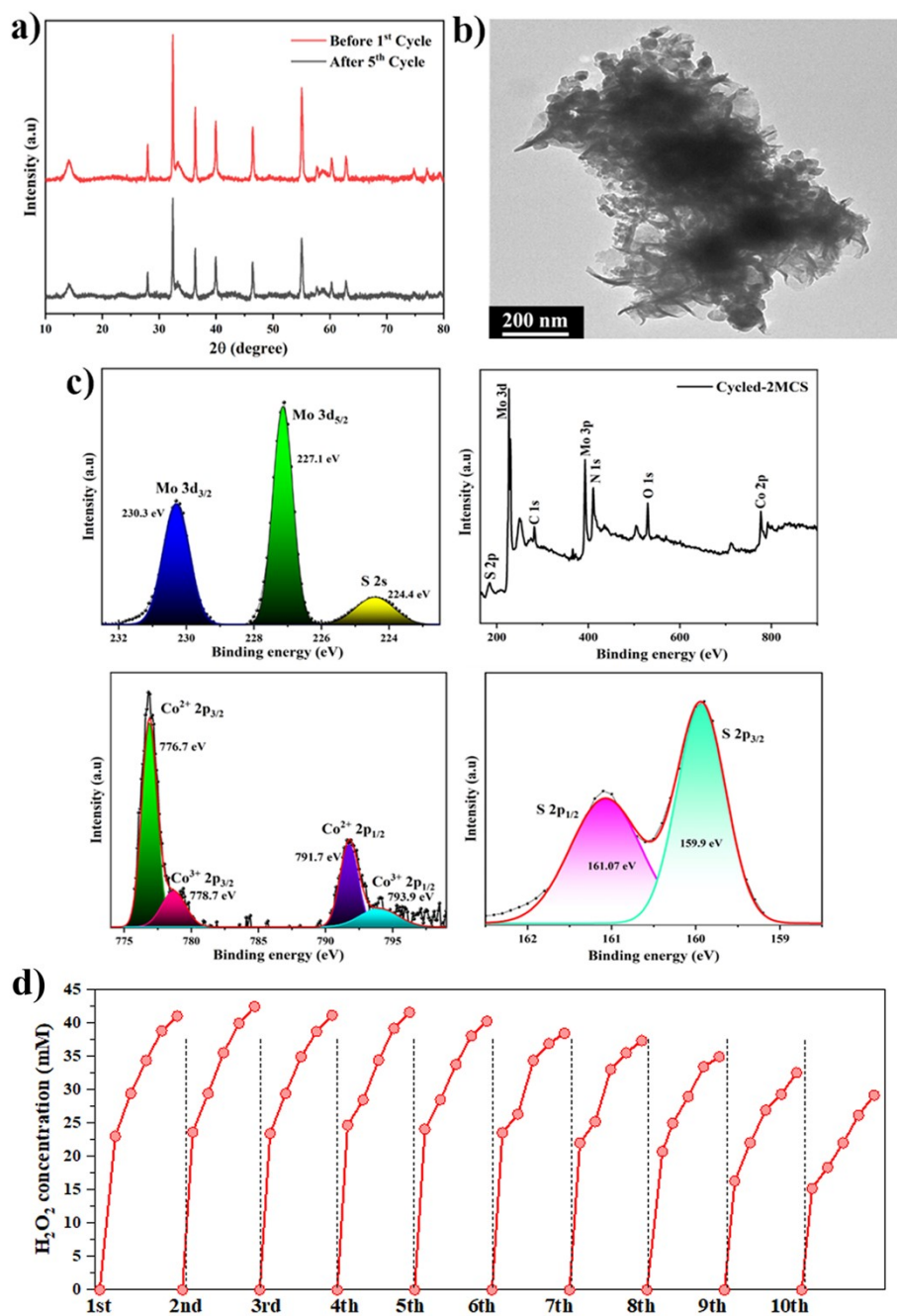


Fig. S6. TE catalyst morphology and structural stability analysis after five cycles (2MCS). (a) XRD spectra, (b) TEM image and (c) XPS spectra of the 2MCS. (d) Ten-cycling test of the 2MCS.

Table S1. Comparison of H₂O₂ production performance with representative photocatalyst, Electrocatalyst and TE catalyst production.

Method of H₂O₂ production	Catalyst	Catalytic conditions	H₂O₂ evolution rates	Refs.
Photocatalysis	TiO ₂ /In ₂ S ₃	300 W Xe lamp	376 μmol h ⁻¹ L ⁻¹	9
	TD-COF	White LED	3364 μmol h ⁻¹ g ⁻¹	10
	TT-COF	White LED	2890 μmol h ⁻¹ g ⁻¹	10
	MIL-125-R7	Visible light	400 μmol h ⁻¹	11
	In ₂ S ₃ @O _v /In ₂ O ₃	Visible-light	275.4 μmol h ⁻¹ g ⁻¹	12
	Bi _{3.6} K ₃ -CN	300 W Xe lamp	402.5 μmolh ⁻¹ L ⁻¹	13
Electrocatalysis	Pd/C fibers	PVA	0.6 mol h ⁻¹ g ⁻¹	14
	Pd/N-doped C	PVA	14.2 mol h ⁻¹ g ⁻¹	15
	Pd-HHDMA ₅ /C	HHDMA	8.4 mol h ⁻¹ g ⁻¹	16
	Au-Pd/TiO ₂	None	110 mol h ⁻¹ g ⁻¹	17
TE catalysis	Bi ₂ Te ₃	ΔT (30) K)	30 μmol L ⁻¹	18
	MoS₂/CoS₂	ΔT (50) K)	39.02 mmol L⁻¹	This work

Notes and references

1. R. Abinaya, S. Harish, S. Ponnusamy, M. Shimomura, M. Navaneethan, M. and J. Archana, *Chem. Eng. J.*, 2021, **416**, 128484.
2. G. Kresse and J. Furthmüller, Efficiency of ab-initio total energy calculations for metals and semiconductors using a plane-wave basis set, *Comput. Mater. Sci.*, 1996, **6**, 15-50.
3. P. E. Blochl, Projector augmented-wave method, *Phys. Rev. B*, 1994, **50**, 17953-17979.
4. G. Kresse and J. Furthmüller, Efficient iterative schemes for ab initio total-energy calculations using a plane-wave basis set, *Phys. Rev. B*, 1996, **54**, 11169.
5. J. P. Perdew, K. Burke and M. Ernzerhof, Generalized Gradient Approximation Made Simple, *Phys. Rev. Lett.*, 1996, **77**, 3865-3868.
6. S. Grimme, J. Antony, S. Ehrlich and H. Krieg, A consistent and accurate ab initio parametrization of density functional dispersion correction (DFT-D) for the 94 elements H-Pu, *J. Chem. Phys.*, 2010, **132**, 154104.
7. V. Wang, N. Xu, J. C. Liu, G. Tang and W. J. C. P. C. Geng, *Compu. Phys. Commun.*, 2021, **267**, 108033.
8. K. Momma and F. Izumi, VESTA3 for three-dimensional visualization of crystal, volumetric and morphology data, *J. Appl. Crystallogr.*, 2011, **44**, 1272-1276.
9. Y. Yang, B. heng and J. Yu, *Nano Research*, 2023, **16**, 4506–4514.
10. J.Y. Yue, L.P. Song, Y.F. Fan, Z.X. Pan, P. Yang, Y. Ma, Q. Xu and B. Tang, 2023, *Angew. Chem*, **62**, 202309624
11. Y. Isaka, Y. Kawase, Y. Kuwahara, K. Mori and H. Yamashita, *Angew. Chem.*, 2019, **131**, 5456-5460.
12. X. Chen, W. Zhang, L. Zhang, L. Feng, C. Zhang, J. Jiang and H. Wang, *ACS Appl. Mater. Interfaces*, 2021, **13**, 25868-25878.
13. H. Liang, A. Wang, R. Cheng, F. Chen, P. Kannan, C. Molochas and P. Tsiakaras, *Chem. Eng. J.*, 2024, **489**, 151145.
14. A. Villa, S.J. Freakley, M. Schiavoni, J.K. Edwards, C. Hammond, G.M. Veith, W. Wang, D. Wang, L. Prati, N. Dimitratos and G.J. Hutchings, *Catal. Sci. Technol.*, 2016, **6**, 694-697.
15. S. Abate, R. Arrigo, M.E. Schuster, S. Perathoner, G. Centi, A. Villa, D. Su and R. Schlögl, *Catal. Today*, 2010, **157**, 280-285.
16. G.M. Lari, B. Puértolas, M. Shahrokhi, N. López and J. Pérez-Ramírez, *Angew. Chem.*, 2017, **129**, 1801-1805.
17. J.K. Edwards, N.E. Ntainjua, A.F. Carley, A.A. Herzing, C.J. Kiely and G.J. Hutchings, *Angew. Chem.*, 2009, **48**, 8512-8515.
18. Y.J. Lin, I. Khan, S. Saha, C.C. Wu, S.R. Barman, F.C. Kao and Z.H. Lin, *Nat. Commun.*, 2021, **12**, 180.